AD-A055 124 ROYAL AIRCRAFT ESTABLISHMENT FARNBOROUGH (ENGLAND) F/G 20/4
LAMINAR FLOW-FIELD COMPUTATION IN AXISYMMETRIC NOZZLES.(U)
NOV 77 B C BARBER

UNCLASSIFIED RAE-TR-77175 DRIC-BR-61832 NL

1 OF 1
AD
A055 124

END
DATE
FILMED
7-78
DDC

TR 77175

ROYAL AIRCRAFT ESTABLISHMENT

*

Technical Report 77175

November 1977

LAMINAR FLOW-FIELD COMPUTATION IN AXISYMMETRIC NOZZLES

by

B.C. Barber

*

Procurement Executive, Ministry of Defence
Farnborough, Hants

UDC 532.517.2 : 532.525 : 533.697.4

ROYAL AIRCRAFT ESTABLISHMENT

Technical Report 77175

Received for printing 29 November 1977

LAMINAR FLOW-FIELD COMPUTATION IN AXISYMMETRIC NOZZLES

by

B. C. Barber

SUMMARY

A numerical procedure for computing the laminar flow-field in nozzles at throat Reynolds numbers of 300-3000 is described. Such nozzles are found in spacecraft position control thrusters, chemical lasers, and low density hypersonic wind-tunnels. A parabolic approximation of the Navier-Stokes equations (the 'boundary layer equations') is transformed to Von Mises form and solved numerically by a central difference method. The entire subsonic and supersonic flow-field is computed. No assumptions or approximations, other than those inherent in the flow equations, are involved. The method is of the direct type and the flow-field for any given nozzle geometry may, in principle, be computed. Examples are given comparing computed results with published experimental data.

Departmental Reference: Space 539

LIST OF CONTENTS

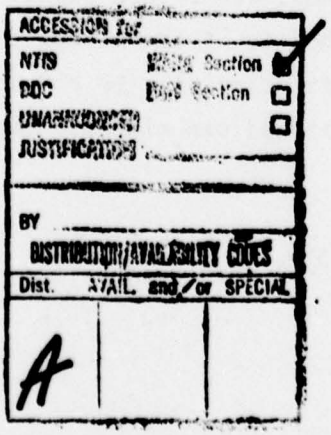

1 INTRODUCTION

Viscous nozzle flows occur in at least three fields of technology. In low thrust satellite position control thrusters the nozzle throat size is of order one millimetre, and typically the throat Reynolds number is in the range 1000-3000. Usually they operate with a propellant of nitrogen, hydrogen or ammonia or mixtures of these gases, often at high temperature. In low density hypersonic wind-tunnels the nozzles are larger, having throat radii from several millimetres to several tens of millimetres and operate with throat Reynolds numbers in a similar range, usually with nitrogen or air[1]. The nozzle walls are often cooled. In chemical lasers the nozzles are of the same size range as satellite control thrusters and operate in the same Reynolds number range, often with fluorine as the 'working fluid'[2].

The numerical procedure described in this Report was developed for predicting the performance of satellite control thrusters. It is, however, equally applicable to any nozzle flow, although in this Report only laminar flows are considered. The basic drawback to operating a convergent-divergent nozzle at laminar Reynolds numbers is that viscous shear forces in the flow in the divergent part of the nozzle inhibit the acceleration of the flow. The boundary layer thus thickens and in extreme cases may encompass the majority of the mass flow. In the case of propulsion nozzles this results in poor nozzle efficiency and a reduction in specific impulse (thrust per unit mass flow). In the case of low density hypersonic wind-tunnel nozzles it limits the obtainable Mach number and limits the region of constant Mach number in the flow core. In the case of chemical lasers the nozzle flow viscous forces reduce the stagnation pressure available for recovery in the laser cavity, and this has a direct bearing on the output power. In addition the reactions which produce the laser power occur between the oxidiser and fuel streams. This is usually limited to the nozzle boundary layer[2] so the influence of the boundary layer on the operation of the laser is important.

Most viscous nozzle flow-field analyses belong to one of two types. In one type of analysis the flow is approximated by a viscous boundary layer and an inviscid core. The flow in the boundary layer may be obtained by using, for example, Cohen and Reshotko's approximate integral method[3] and then using an iterative technique to couple the boundary layer and inviscid core. This approach was followed by Murch *et al*[4] and by Potter and Carden[5]. Alternatively, the equations of the boundary layer may be transformed by introducing a

175

stream-function and applying a modification of the Lees-Dorodnitsyn transformation (a combination of the Mangler transformation and Illingworth transformation).

The resulting coupled pair of partial differential equations may then be solved directly by a finite difference procedure (Whitfield[6]) or the equations may be simplified and transformed to a pair of ordinary differential equations by assuming local similarity. These equations may then be solved more readily at the expense of the constraints imposed by similarity. This approach was adopted by Edwards[7]. In both cases the boundary layer solutions are coupled iteratively to the one-dimensional core flow.

In the other type of analysis the entire flow-field is computed by solving the Navier-Stokes equations directly. Only one analysis of this type has been reported[8]. Here, Rae solved a parabolic approximation of the Navier-Stokes equations (the 'boundary layer equations') in the channel flow approximation[9] for the whole flow-field. An implicit Crank-Nicholson finite difference scheme was used.

At low Reynolds numbers experimental evidence[10] indicates that the inviscid core almost disappears. The viscous boundary layer-inviscid core approximation is then not even approximately true. It then becomes very desirable to account for the viscous effects over the whole flow, and an analysis of the complete flow-field becomes necessary. It is assumed, of course, that the Reynolds numbers are not so low that the Navier-Stokes equations cease to be valid.

A difficulty with the channel flow approximation is that the channel walls are limited to small angles of convergence and divergence. Furthermore, no account is taken of any radial pressure gradient. In general the streamtubes are inclined to the symmetry axis. There will thus be a component of the pressure gradient along the streamtubes in the radial direction, and experimental data in Ref 10 shows that this component may not be ignored.

The numerical analysis reported here is of the 'entire flow-field computation' type. The nozzle flow-field is computed using a form of the boundary layer equations in which a radial pressure gradient exists.

2 THE FLOW EQUATIONS

The starting point is the form of the boundary layer equations developed by Probstein and Elliott[11]. These equations were also used by Whitfield[6] and

by Edwards[7]. Symbols are defined in the nomenclature. The coordinate system is shown in Fig 1.

$$\rho u \frac{\partial u}{\partial x} + \rho v \frac{\partial u}{\partial y} = - \frac{dp}{dx} + \frac{1}{r} \frac{\partial}{\partial y} \left(r\mu \frac{\partial u}{\partial y} \right) \tag{1}$$

$$\rho u \frac{\partial h}{\partial x} + \rho v \frac{\partial h}{\partial y} = u \frac{dp}{dx} + \frac{1}{r} \frac{\partial}{\partial y} \left(r \frac{k}{C_p} \frac{\partial h}{\partial y} \right) + \mu \left(\frac{\partial u}{\partial y} \right)^2 \tag{2}$$

$$\frac{\partial}{\partial x} (\rho u r) + \frac{\partial}{\partial y} (\rho v r) = 0 \tag{3}$$

$$\frac{\partial p}{\partial y} = 0 \tag{4}$$

where ρ is the density, h is the static enthalpy, p the static pressure, μ the laminar viscosity, k the thermal conductivity, C_p the specific heat at constant pressure, u the velocity in the longitudinal direction, v the velocity in the transverse direction, x the longitudinal coordinate, y the transverse coordinate, and r is the radius.

Probstein and Elliott derived these equations for external flow where the boundary layer thickness is much smaller than the longitudinal radius of curvature. These equations are here extended to internal flow and to the whole of the flow-field. The distance x is measured from some reference plane along a given streamtube and the distance y is measured from the symmetry axis along a surface orthogonal to the streamtubes. In this case this is also a surface of constant static pressure since the transverse momentum equation is neglected leading to $\partial p/\partial y = 0$. In this approximation this arises from neglecting the centrepetal force component which accompanies a change in direction of the flow, *ie* $\partial\theta/\partial x$ is assumed negligible. This is a good approximation in the divergent part of the nozzle where the streamtubes are only slightly curved, but in the region of the nozzle throat this approximation is not so satisfactory.

The equations are thus not limited to small angles of convergence and divergence of the nozzle walls, but are limited to small first derivatives. In this sense this approximation is one order higher than that used by Rae[8] and there is a radial component of the pressure gradient.

2.1 Transformation of the flow equations

Equation (3) may be written in parametric form:

$$\rho u r = \frac{\partial \psi}{\partial y} \tag{5}$$

$$\rho v r = -\frac{\partial \psi}{\partial x} \tag{6}$$

where the parameter ψ is the compressible stream function[12]. From the chain rule for differentiation we have the following operators:

$$\left(\frac{\partial}{\partial x}\right)_y = \left(\frac{\partial}{\partial x}\right)_\psi + \left(\frac{\partial \psi}{\partial x}\right)_y \left(\frac{\partial}{\partial \psi}\right)_x \tag{7}$$

$$\left(\frac{\partial}{\partial y}\right)_x = \left(\frac{\partial \psi}{\partial y}\right)_x \left(\frac{\partial}{\partial \psi}\right)_x \tag{8}$$

so that

$$\left(\frac{\partial}{\partial x}\right)_y = \left(\frac{\partial}{\partial x}\right)_\psi - \rho v r \left(\frac{\partial}{\partial \psi}\right)_x \tag{9}$$

$$\left(\frac{\partial}{\partial y}\right)_x = \rho u r \left(\frac{\partial}{\partial \psi}\right)_x \, . \tag{10}$$

Thus equations (1) and (2) may be transformed from coordinates x, y to x, ψ and we have:

$$\frac{\partial u}{\partial x} = -\frac{1}{\rho u}\frac{dp}{dx} + \frac{\partial}{\partial \psi}\left(\mu \rho u r^2 \frac{\partial u}{\partial \psi}\right) \tag{11}$$

$$\frac{\partial h}{\partial x} = \frac{1}{\rho}\frac{dp}{dx} + \frac{\partial}{\partial \psi}\left(\rho u r^2 \frac{k}{C_p}\frac{\partial h}{\partial \psi}\right) + \mu \rho u r^2 \left(\frac{\partial u}{\partial \psi}\right)^2 \, . \tag{12}$$

This is known as Von Mises transformation[13].

The value of ψ at the axis of the nozzle is taken to be zero (an arbitrary, but convenient, choice). At the nozzle wall:

$$\psi_w = \int_0^{y_w} \rho u r \, dy \tag{13}$$

and is independent of x since the total mass flow is conserved throughout the nozzle. Hence:

$$\psi_w = \dot{m}/2\pi \tag{14}$$

where $\dot{m}$ is the total mass flow rate.

It is known that in the Von Mises form the boundary layer equations are likely to lead to a more stable numerical procedure[14]. In addition they may be solved numerically by a marching integration procedure which avoids any iteration as will be shown later.

This method of handling the boundary layer equations is essentially the same as that employed by Patankar and Spalding for general second order parabolic equations[15].

Equations (11) and (12) are written in terms of non-dimensional variables (defined in the nomenclature) and become:

$$\frac{\partial u^*}{\partial x^*} = -\frac{1}{\gamma_0 M_0^2}\frac{1}{\rho^* u^*}\frac{dp^*}{dx^*} + 8Pr_0\frac{\partial}{\partial \psi^*}\left(\mu^*\rho^* u^* r^{*2}\frac{\partial u^*}{\partial \psi^*}\right) \tag{15}$$

$$\frac{\partial h^*}{\partial x^*} = \frac{\gamma_0 - 1}{\gamma_0}\frac{1}{\rho^*}\frac{dp^*}{dx^*} + 8\frac{\partial}{\partial \psi^*}\left(\rho^* u^* r^{*2}\frac{k^*}{C_p^*}\frac{\partial h^*}{\partial \psi^*}\right) + 8Pr_0 M_0^2(\gamma_0 - 1)\,\mu^*\rho^* u^* r^{*2}\left(\frac{\partial u^*}{\partial \psi^*}\right)^2 \tag{16}$$

where M is the Mach number, γ the ratio of specific heats and Pr is the Prandtl number. The superscript (*) refers to non-dimensional variables and the subscript (0) refers to mean values at the duct entrance.

2.2 The boundary conditions

An idea of the nozzle geometry may be gained from Fig 3 or Fig 6. It will be seen that at the nozzle inlet the wall is parallel with the symmetry axis. It is assumed that at the nozzle inlet the flow has constant enthalpy across its cross-section and that a fully established (parabolic) velocity profile exists. It is further assumed that there is no radial velocity component. Thus we have:

$$u^* = 2(1 - \psi^*)^{\frac{1}{2}}, \quad v^* = 0, \quad h^* = 1 \quad \text{at} \quad x^* = 0. \tag{17}$$

At the nozzle axis the conditions express the symmetry. So we have:

$$\frac{\partial u^*}{\partial \psi^*} = 0 , \quad v^* = 0 , \quad \frac{\partial h^*}{\partial \psi} = 0 \quad \text{at} \quad \psi^* = 0 . \tag{18}$$

It is assumed that at the nozzle wall non-slip conditions are appropriate, *ie* velocity slip and temperature jump are ignored. Hence:

$$u^* = 0 , \quad v^* = 0 , \quad \frac{\partial h^*}{\partial y^*} = \frac{C_p^* q^*}{k^*} \quad \text{at} \quad \psi^* = 1 \tag{19}$$

where q^* is the non-dimensional heat flux at the nozzle wall.

For the two test cases presented in section 5 the wall was assumed to be adiabatic, *ie* $q^* = 0$. Note that the transverse enthalpy gradient is left in terms of the transverse coordinate y^* . The reason for this is that as $y \to y_w$, $\partial h/\partial \psi \to \infty$ because $u \to 0$ and it is possible to incorporate the boundary conditions as shown and thus avoid the singularity.

3 THE GAS PROPERTIES

The computations presented in this Report were performed with nitrogen. The equation of state used is:

$$p = \rho RT/m \tag{20}$$

where $R = 8.3143 \times 10^3$ J K^{-1} kg-mole^{-1}
and $m = 28.013$ (the molecular weight).
The gas is thus assumed to be 'ideal'.
The Prandtl number was assumed constant at $Pr = 0.7$.
The viscosity was assumed to obey Sutherland's law:

$$\mu = \frac{14.5\ T^{3/2}}{122.0 + T} \times 10^{-7} \text{ N s/m}^2 . \tag{21}$$

The specific heat is assumed constant at $C_p = 1.0397 \times 10^3$ J kg^{-1} K^{-1} and the ratio of specific heats, $\gamma = 1.400$.

It is assumed that all energy states are in mutual equilibrium and frozen flow losses are ignored.

4 THE FINITE DIFFERENCE PROCEDURE

Equations (15) and (16), together with the initial and boundary conditions (17) to (19), the equation of state (20) and the viscosity law (21) and various mainly geometrical relationships (which will be developed in section 4.3) form the starting point for the numerical procedure.

A central difference technique is used to solve equations (15) and (16). A general point in the mesh scheme and the domain of integration in the $x^* - \psi^*$ plane is shown in Fig 2. The equations have been integrated up to and including the mth axial point and the solution is about to be extended to the m + 1th axial point; ϕ is an arbitrary function and B is an arbitrary coefficient. Thus we have:

$$\frac{\partial \phi}{\partial x^*} = \frac{\phi_{m+1,n} - \phi_{m,n}}{\Delta x^*} \tag{22}$$

$$\frac{\partial \phi}{\partial \psi^*} = \frac{1}{2\Delta\psi^*}\left(\phi_{m+1,n+1} - \phi_{m+1,n-1}\right) \tag{23}$$

$$\frac{\partial}{\partial \psi^*}\, B\, \frac{\partial \phi}{\partial \psi^*} = \frac{1}{\Delta\psi^*}\left\{\frac{\left(B_{m,n+1} + B_{m,n}\right)\left(\phi_{m+1,n+1} - \phi_{m+1,n}\right)}{2\Delta\psi^*} - \frac{\left(B_{m,n} + B_{m,n-1}\right)\left(\phi_{m+1,n} - \phi_{m+1,n-1}\right)}{2\Delta\psi^*}\right\}. \tag{24}$$

The Crank-Nicolson scheme is sometimes not stable for flow in a duct[14,16] so a fully implicit scheme is used and values of ϕ are evaluated along the line m + 1. Values of the arbitrary coefficient B are taken along the m line where the previous solution is known. This avoids non-linearity and the resulting necessity for iteration.

Equations (15) and (16) may be written in the form:

$$\frac{\partial \phi}{\partial x^*} = A\,\frac{dp^*}{dx^*} + \frac{\partial}{\partial \psi^*}\left(B\,\frac{\partial \phi}{\partial \psi^*}\right) + C \tag{25}$$

for $\phi \equiv u^*$ we have:

$$A \equiv -\frac{1}{\gamma_0 M_0^2}\,\frac{1}{\rho^* u^*} \tag{26}$$

$$B \equiv 8Pr_0 \mu^*\rho^*u^*r^{*2} \tag{27}$$

$$C \equiv 0 \tag{28}$$

for $\phi \equiv h^*$:

$$A \equiv \frac{\gamma_0 - 1}{\gamma_0} \frac{1}{\rho^*} \tag{29}$$

$$B \equiv 8\rho^*u^*r^{*2} \frac{k^*}{C_p^*} \tag{30}$$

$$C \equiv 8Pr_0M_0^2(\gamma_0 - 1) \frac{\mu^*\rho^*u^*r^{*2}}{4(\Delta\psi^*)^2} \left(u^*_{m,n+1} - u^*_{m,n-1}\right)^2 . \tag{31}$$

Note that in equation (16) $\partial u^*/\partial\psi^*$ is evaluated along the m line:

$$\left(\frac{\partial u^*}{\partial\psi^*}\right)^2 = \frac{1}{4(\Delta\psi^*)^2} \left(u^*_{m,n+1} - u^*_{m,n-1}\right)^2 . \tag{32}$$

In each case the coefficients A, B and C are evaluated on the basis of the known solution at the previous step. They are therefore regarded as constants.

4.1 The flow equations in finite difference form

Writing (25) in finite difference form using (22) and (24) we have:

$$\phi_{m+1,n-1}\left\{-\frac{\Delta x^*}{2(\Delta\psi^*)^2}\left(B_{m,n} + B_{m,n-1}\right)\right\}$$

$$+ \phi_{m+1,n}\left\{1 + \frac{\Delta x^*}{2(\Delta\psi^*)^2}\left(B_{m,n+1} + 2B_{m,n} + B_{m,n-1}\right)\right\}$$

$$+ \phi_{m+1,n+1}\left\{-\frac{\Delta x^*}{2(\Delta\psi^*)^2}\left(B_{m,n} + B_{m,n+1}\right)\right\}$$

$$= A_{m,n}\Delta p^* + \Delta x^* C_{m,n} + \phi_{m,n} . \tag{33}$$

Let:

$$c_{i,i} = -\frac{\Delta x^*}{2(\Delta\psi^*)^2}\left(B_{m,i+1} + B_{m,i}\right) \tag{34}$$

$$c_{i,i+1} = 1 + \frac{\Delta x^*}{2(\Delta\psi^*)^2}\left(B_{m,i+2} + 2B_{m,i+1} + B_{m,i}\right) \tag{35}$$

$$c_{i,i+2} = -\frac{\Delta x^*}{2(\Delta\psi^*)^2}\left(B_{m,i+1} + B_{m,i+2}\right) \quad . \tag{36}$$

Then we have:

$$\begin{bmatrix} c_{11} & c_{12} & c_{13} & & & \\ & c_{22} & c_{23} & c_{24} & & \\ & & \ddots & \ddots & \ddots & \\ & & & c_{N-1,N-1} & c_{N-1,N} & c_{N-1,N+1} \end{bmatrix} \begin{bmatrix} \phi_{m+1,1} \\ \\ \\ \phi_{m+1,N+1} \end{bmatrix} = \begin{bmatrix} b_1 \\ \\ \\ b_{N-1} \end{bmatrix} \tag{37}$$

where $$b_i = A_{m,i}\Delta p^* + \Delta x^* C_{m,i} + \phi_{m,i} \quad . \tag{38}$$

Note that the flow has been divided into N equal movements of stream function:

$$\Delta\psi^* = 1/N \tag{39}$$

(37) gives a system of $N-1$ equations in $N+1$ unknowns.

4.2 The boundary conditions

The boundary conditions give zero gradient of ϕ at the symmetry axis. So $\phi_{m+1,1} = \phi_{m+1,2}$ and c_{11} may be added to c_{12}, the first column deleted from the coefficient matrix in (37), and $\phi_{m+1,1}$ deleted. The boundary conditions at the nozzle wall are of two types. Either the value of ϕ is specified or its first derivative. When $\phi \equiv u^*$ the first of these alternatives applies and we have $\phi_{m+1,N+1} = 0$. In this case the last column may be deleted from the coefficient matrix and $\phi_{m+1,N+1}$ deleted. When $\phi \equiv h^*$, and an adiabatic wall is assumed we have $\phi_{m+1,N} = \phi_{m+1,N+1}$ so that $c_{N-1,N+1}$ may be added to $c_{N-1,N}$, the last column deleted from the equations and $\phi_{m+1,N+1}$ deleted. The effect is the same in both instances; the coefficient matrix is reduced to tridiagonal form and we have $N-1$ equations in $N-1$ unknowns:

175

$$\begin{bmatrix} (c_{11} + c_{12}) & c_{13} & & & \\ & c_{22} & c_{23} & c_{24} & \\ & \ddots & \ddots & \ddots & \ddots \\ & & c_{N-2,N-2} & c_{N-2,N-1} & c_{N-2,N} \\ & & & c_{N-1,N-1} & (c_{N-1,N} + c_{N-1,N+1}) \end{bmatrix} \begin{bmatrix} \phi_{m+1,2} \\ \\ \\ \\ \phi_{m+1,N} \end{bmatrix} = \begin{bmatrix} b_1 \\ \\ \\ \\ b_{N-1} \end{bmatrix} . \quad (40)$$

Other conditions at the nozzle wall may be treated in a similar way. If ϕ is specified and is other than zero (for example the wall temperature may be given, or the velocity, if a velocity jump is allowed), then the term $c_{N-1,N+1}\phi_{m+1,N+1}$ may be subtracted from b_{N-1} and the last column deleted and $\phi_{m+1,N+1}$ deleted.

The case where a finite gradient is specified is a little more involved. For example suppose the heat flux is given. Then at the nozzle wall:

$$\frac{\partial h^*}{\partial y^*} = \frac{c_p^*}{k^*} q^* \quad (41)$$

and also

$$\frac{\partial h}{\partial y} = \rho u r \frac{\partial h}{\partial \psi} \quad (42)$$

so that

$$\frac{\partial h^*}{\partial y^*} = 2\rho^* u^* r^* \frac{\partial h^*}{\partial \psi^*} . \quad (43)$$

Hence

$$\frac{\partial h^*}{\partial \psi^*} = \frac{Prq^*}{2\mu^*\rho^* u^* r^*} . \quad (44)$$

In finite difference form:

$$h^*_{m+1,N+1} - h^*_{m+1,N} = \frac{8\Delta\psi^* q^* Pr}{\left(\mu^*_{m,N+1} + \mu^*_{m,N}\right)\left(\rho^*_{m,N+1} + \rho^*_{m,N}\right)\left(u^*_{m,N+1} + u^*_{m,N}\right)\left(r^*_{m,N+1} + r^*_{m,N}\right)} \quad \ldots\ldots(45)$$

The RHS is known on the basis of the previous step. So $h^*_{m,N+1}$ may be expressed in terms of $h^*_{m+1,N}$ and the coefficient matrix reduced as before.

4.3 Solution of the finite difference equations

The two tridiagonal systems of equations for u^* and h^* are solved at each step by a Gaussian elimination method[17]. For a tridiagonal system of equations this results in a very compact procedure.

The temperature vector is computed from the enthalpy vector, and the density vector from the temperature and pressure.

The radial coordinate is computed from a recurrence relation:

$$\rho u r = \frac{\partial \psi}{\partial y} \tag{46}$$

so

$$\frac{\partial \psi^*}{\partial y^*} = 2\rho^* u^* r^* \quad . \tag{47}$$

It is easily shown from the geometry that

$$\frac{\partial r^*}{\partial y^*} = \cos\theta \tag{48}$$

so

$$\frac{\partial \psi^*}{\partial r^*} = \frac{2\rho^* u^* r^*}{\cos\theta} \quad . \tag{49}$$

In finite difference form:

$$\Delta r^* = r^*_{n+1} - r^*_n = \frac{4\Delta\psi^* \cos\theta_{n+1}}{\left(\rho^*_n + \rho^*_{n+1}\right)\left(u^*_n + u^*_{n+1}\right)\left(r^*_n + r^*_{n+1}\right)} \quad . \tag{50}$$

Hence:

$$r^*_{n+1} = \sqrt{r^{*2}_n + \frac{4\Delta\psi^* \cos\theta_{n+1}}{\left(\rho^*_n + \rho^*_{n+1}\right)\left(u^*_n + u^*_{n+1}\right)}} \quad . \tag{51}$$

Thus given that $r_1^* = 0$ and values for the density, velocity and streamtube inclination at the previous step the radii may be easily computed.

In general the final radius r_{N+1}^* does not quite coincide with the duct wall, *ie* the computed flow-field does not quite fit the duct. This is because the procedure uses the pressure and pressure gradient computed at the previous step. The procedure corrects the pressure to make the computed flow-field fit the duct and the resulting pressure and pressure gradient are used at the next axial step. Thus no iteration is required, the procedure simply marches along the nozzle, the pressure and pressure gradient being controlled by an error parameter. The necessary correction to the pressure is estimated from the one-dimensional flow equation connecting pressure change and area change[18]:

$$\frac{dp}{p} = \frac{\gamma M^2}{1 - M^2} \frac{dA}{A} \quad . \tag{52}$$

The mean Mach number across the flow is used and the area change is computed from the radius error. It was found desirable to use only a fraction of the pressure correction to ensure stability. In addition the magnitude of the correction must be limited to avoid problems with the singularity at M = 1.

Because the radii fluctuate the streamtube inclination also fluctuates, and this is coupled back into the equations and produces instability. In order to overcome this effect a small step length is used (1/250 of the throat radius) and the change in inclination is computed every 7-25 steps depending on the wall curvature. In regions of high curvature the smaller interval was used since the radius is changing more rapidly and small errors have less effect on the inclination. The effect is to smooth the streamlines, and it successfully stabilises the procedure at the expense of greatly reducing its efficiency.

The streamtube inclination θ is calculated from the geometry. We have:

$$\sin \theta = \frac{\Delta r}{\Delta x} \tag{53}$$

where Δr is the change in radius from the chosen point 7-25 steps upstream, to the current point along a given streamtube. Δx is the corresponding change in longitudinal distance. The expression becomes increasingly inaccurate as $\partial\theta/\partial x$ increases. It can, however, be shown to be consistent with the other assumptions, specifically $\partial p/\partial \psi = 0$.

If the flow parameters are such that the flow does not choke at the nozzle throat the pressure decreases up to the nozzle throat, and then increases the flow being everywhere subsonic. If the procedure tries to force too great a mass flow through the nozzle it fails; the flow chokes before the throat is reached. When this situation occurs the error between the computed flow-field and the duct radius increases rapidly, resulting in a greatly increased negative pressure gradient. The pressure then becomes negative and the procedure fails. Both these situations may be easily detected and upper and lower bounds on the mass flow rate established. The procedure then takes the mean of the upper and lower bounds and establishes a new upper or lower bound depending whether the new mass flow rate leads to premature choking or no choking. Thus the flow rate is adjusted until the flow chokes at the nozzle throat and then the pressure decreases monotonically throughout the duct. This bisection method of iteration has only linear convergence, but convergence is guaranteed and usually only about eight iterations required. This point is explained further in the next paragraph.

The eigenstate corresponding to choking is not well defined. If the mass flow rate is slightly greater than the 'true' eigenvalue the computed flow-field expands slightly in the region of the throat, to accommodate it. The sonic surface then intersects the nozzle axis slightly upstream of the geometric throat. If the mass flow is very carefully adjusted to make the error parameter a minimum in the throat region the sonic surface intersects the axis slightly downstream of the geometric throat. It is thus possible to make the sonic surface intersect the axis at any arbitrary point (within limits) around the nozzle throat. It is possible to vary the mass flow by about 0.5% at a throat Reynolds number of 2000 and achieve a smooth expansion to supersonic flow. At a Reynolds number of 500 the flow is more critical and it is possible to vary the flow only by about 0.05%. This phenomenon is a result of the numerical method used, at least in part. Rae[8] also noted a similar effect, except that his mass flow was much better defined and the limits between which the sonic surface could be varied were both downstream of the nozzle throat. The effect is very convenient from the practical standpoint. It means that when the whole procedure is iterated to find the choking eigenstate it is only necessary to find the mass flow rate to three significant figures, which saves time.

Note that no additional assumptions or fitting (as was done in Ref 8) is
175 required in the region of the singularity at the throat. When the choking mass

flow rate has been determined the procedure will start from its initial conditions and continue to compute through the subsonic flow through the throat and into the supersonic flow in the expansion cone.

The computations presented in this Report were performed in single precision - seven significant figures - on a large minicomputer. Double precision made no significant difference to the results. The procedure is very inefficient and for the two test cases presented the total time for each was about 4 hours. This is a total of eight iterations of the flow up to the throat to determine the eigenstate and one complete determinator of the flow to the nozzle exit. This time is reduced to a total of about 20 minutes using a more modern computer (PRIME 400). Thus although procedures such as the one described in this Report are very lengthy the advent of modern fast computers means that they become more practicable.

5 RESULTS

A survey of the literature reveals little detailed experimental data on the flow-fields in low density nozzle flows. The exception is Ref 10. Here, Rothe measured the gas density and temperature at a large number of points throughout the flow of nitrogen through small nozzles using an electron beam fluorescence technique. His measurements covered throat Reynolds numbers (based on throat diameter) from 639 down to 57.

Two of the nozzle flows presented in Ref 10 were chosen as test cases for the present work. In both examples the 'propellant' is nitrogen at an initial temperature of 300 K. Also in both examples the semi-angle of the convergent part of the nozzle is 30°, the semi-angle of the nozzle expansion cone is 20° and the longitudinal radius of curvature of the throat is one half the transverse radius. For the purposes of this computation the radius of the inlet was taken to be three times the throat radius.

5.1 Example 1

The throat Reynolds number (based on diameter) = 639 and the throat diameter = 2.50 mm, the inlet pressure = 1.981×10^{3} N/m^{2} (1.955×10^{-2} bar) and the mass flow rate = 20.1 mg/s. The computed flow-field is shown in Fig 3. The lower half of the nozzle shows the streamtubes and orthogonal (constant pressure) surfaces. The upper half shows the displacement thickness and constant Mach surfaces at M = 1, 2, 3 and 4. The computation was performed with 20 streamtubes although only 10 are shown for clarity.

It will be noted that the displacement thickness is compressed considerably by the convergent part of the nozzle, but grows out into the stream in the expansion cone. Although about 95% of the mass flow becomes sonic only about 70% is accelerated to Mach 3.

It is unsafe to make conclusions of an analytic nature from a numerical analysis, especially in the region of singularities, but the behaviour of the sonic surface at the nozzle throat may be compared with the sonic surface in two-dimensional inviscid flow. In inviscid flow the sonic surface is parabolic in form near the symmetry axis, intersects the axis downstream of the geometric throat and is concave towards the flow (see for example Ref 19). Here the sonic surface is slightly convex towards the flow.

The axial static temperature is shown in Fig 4. Near the throat the agreement with experimental results is excellent and even near the exit plane the computed curve is only just outside the error bars. Fig 5 shows the results for the axial static pressure. The computed curve agrees with the experimental curve to within 20%.

5.2 Example 2

The throat Reynolds number = 307 and the throat diameter = 5.1 mm, the inlet pressure = 4.657×10^{2} N/m^{2} (4.596×10^{-3} bar) and the mass flow rate 18.97 mg/s.

The computed flow-field is shown in Fig 6. The displacement thickness curves more rapidly into the flow in the expansion cone and only about 45% of the mass flow is accelerated to M = 3.

The axial static temperature is plotted in Fig 7 and here again the agreement with experimental results is good. Note the oscillation in the curve at X/R_t = 17 due to an incipient instability. Fig 8 shows the axial static pressure and here the agreement is excellent except for the oscillation near X/R_t = 17. The cause of this oscillation has not yet been identified. A further example at a lower Reynolds number (91) was tried, but increased instability prevented a reliable computation.

In the present case Rothe presents results for the radial profiles of temperature, density and pressure at X/R_t = 13.7. Fig 9 shows the radial static temperature. The computed results are within or on the edge of the error bars over the whole range. In Fig 10 the radial density profiles are shown, here the agreement is not so good but still reasonable. Fig 11 shows the radial pressure

175

profile and here the agreement is poor. At the nozzle wall the computed pressure loss is about 12%, but the measured loss is about 29.5%. Fig 6 shows that the streamtubes are only very slightly curved in this region so that the extra pressure loss is unlikely to be caused by a centrepetal force component, and in any event the streamtubes are curved towards the symmetry axis which would tend to increase the pressure along the radius. It is tempting to speculate that the pressure effect is caused by the influence of the low pressure in the vacuum chamber in which the nozzle is tested, being propagated upstream through the subsonic part of the flow. The procedure described in this Report, being based on a parabolic approximation, is unable to take this kind of effect into account.

6 CONCLUSIONS

The object of the work presented in this Report was to develop a numerical procedure suitable for computing the entire flow-field in a nozzle at low Reynolds numbers. As the results in examples 1 and 2 show this has been reasonably successful. No approximations are required other than those inherent in the boundary layer equations. Similarity is not assumed. A viscous boundary layer - inviscid cone flow is not assumed. Furthermore the method is of the direct type, the flow can be computed from a given nozzle geometry.

Despite the low density of the flow in the examples, non-slip boundary conditions were employed and gave reasonable results.

A criticism sometimes levelled at full flow-field computations is that they are slow and require large fast computers. This may have been true in the past, but computers are becoming more powerful, so much so that procedures of the type described here are now practicable propositions.

Acknowledgment

The author thanks Dr P.D. Smith, Aerodynamics Department, Bedford, for his helpful criticism.

NOMENCLATURE

A	arbitrary coefficient in equation (30), defined in identities 31 and 34, or area in equation (60)
a	radius of nozzle wall
a_0	radius of nozzle inlet
a_t	radius of nozzle throat
B	arbitrary coefficient in equations (28) and (30), defined in identities 32 and 35
b	defined in equation (42)
C	arbitrary coefficient in equation (30), defined in identities 33 and 36
C_p	specific heat at constant pressure
C_p^*	C_p/C_{p_0}
c	matrix coefficient defined in equations (38), (39) and (40)
h	static enthalpy ($\Delta h = C_p \Delta T$)
h*	h/h_0
k	thermal conductivity
k*	k/k_0
M	Mach number
m	molecular weight
$\dot{m}$	mass flow rate
N	number of streamtubes
p	static pressure
p*	p/p_0
Pr	Prandtl number $\mu C_p/k$
q	heat flux at nozzle wall
q*	qa_0/k_0T_0
R	gas constant
Re	Reynolds number $2a(\rho u)_{mean}/\mu$
r	radius
r*	r/a_0
T	static temperature
u	velocity in longitudinal direction
u*	u/u_0

175

NOMENCLATURE (concluded)

v	velocity in transverse direction
X	x/a_t , x measured along symmetry axis from nozzle throat
x	coordinate in longitudinal direction
x*	$(x/a_0)/Pr_0Re_0$
y	coordinate in transverse direction
y*	y/a_0
γ	ratio of specific heats
Δ	finite difference
θ	streamtube inclination
μ	viscosity
μ^*	μ/μ_0
ρ	density
ρ^*	ρ/ρ_0
ϕ	arbitrary function
ψ	stream function
ψ^*	$\psi 2\pi/\dot{m}$

Subscripts

m	denotes arbitrary point in x direction
mean	denotes mean value
n	denotes arbitrary point in ψ direction
0	denotes initial conditions
w	denotes value at nozzle wall

Superscripts

*	denotes non-dimensional variable

REFERENCES

No.	Author	Title, etc
1	D.L. Whitfield	Theoretical and experimental investigation of boundary layers in low density hypersonic axisymmetric nozzles. Arnold Engineering Development Center TR-68-183 (1968)
2	R.J. Driscoll	Study of the boundary layers in chemical laser nozzles. AIAA J. Vol 14, 11, pp 1571-1577 (1976)
3	C.B. Cohen E. Reshotko	The compressible laminar boundary layer with heat transfer and arbitrary pressure gradient. NACA Report 1294 (1956)
4	C.K. Murch *et al*	Low thrust nozzle performance. AIAA paper 68-91 (1968)
5	J.L. Potter W.H. Carden	Design of axisymmetric contoured nozzles for laminar hypersonic flow. J. Spacecraft and Rockets, Vol 5, pp 1095-1100 (1968)
6	D.L. Whitfield C.H. Lewis	Boundary layer analysis of low density nozzles including displacement slip and transverse curvature. J. Spacecraft and Rockets, Vol 7, pp 462-468 (1970)
7	I. Edwards	A theoretical study of the performance of resistojet nozzles. PhD thesis, University of Southampton (1972)
8	W.J. Rae	Study of low density nozzle flows, with application to microthrust rockets. NASA-CR-107299, accession No.N75-70145 (Cornell Aeronautical Lab) Also published in:
	W.J. Rae	Some numerical results on viscous low density nozzle flows in the slender channel approximation. AIAA J., Vol 9, pp 811-820 (1971)

REFERENCES (continued)

No.	Author	Title, etc
9	J.C. Williams	Viscous compressible and incompressible flow in slender channels. AIAA J., Vol 1, 1, pp 186-195 (1963)
10	D.E. Rothe	Experimental study of viscous low-density nozzle flows. Cornell Aeronautical Lab Report AI-2590-A-2 (1970) Also published in:
	D.E. Rothe	Electron beam studies of viscous flow in supersonic nozzles. AIAA J., Vol 9, pp 804-811 (1971)
11	R.F. Probstein D. Elliott	The transverse curvature effect in compressible axially symmetric laminar boundary layer flow. J. of the Aeronautical Sciences, Vol 23, pp 208-224 and 236 (1956)
12	Th Von Kármán H.S. Tsien	Boundary layer in compressible fluids. J. of the Aeronautical Sciences, Vol 5, pp 227-232 (1938)
13	H. Schlichting	Boundary layer theory. Pergamon (1965)
14	M.R. Abbott	Axially symmetric steady motion of a viscous incompressible fluid: some numerical experiments. RAE Technical Note Math 98 (1963)
15	S.V. Patankar D.B. Spalding	A finite difference procedure for solving the equations of the two-dimensional boundary layer. Int J Heat and Mass Transfer, Vol 10, pp 1387-1411 (1967)
16	P.M. Worsoë-Schmidt G. Leppert	Heat transfer and friction for laminar flow of gas in a circular tube at high heating rate. Int J Heat and Mass Transfer, Vol 8, pp 1281-1301 (1965)

REFERENCES (concluded)

No.	Author	Title, etc
17	B. Carnaham H.A. Luther J.O. Wilkes	Applied numerical methods. J. Wiley and Sons Ltd (1969)
18	A.H. Shapiro W.R. Hawthorne	The mechanics and thermodynamics of one-dimensional gas flow. J. App. Mech, Vol 14, 4, pp A317-A336 (1947)
19	I.M. Hall	Transonic flow in two-dimensional and axially symmetric nozzles. Quart J. Mech and App. Math., Vol 15, part 4, pp 487-508 (1962)

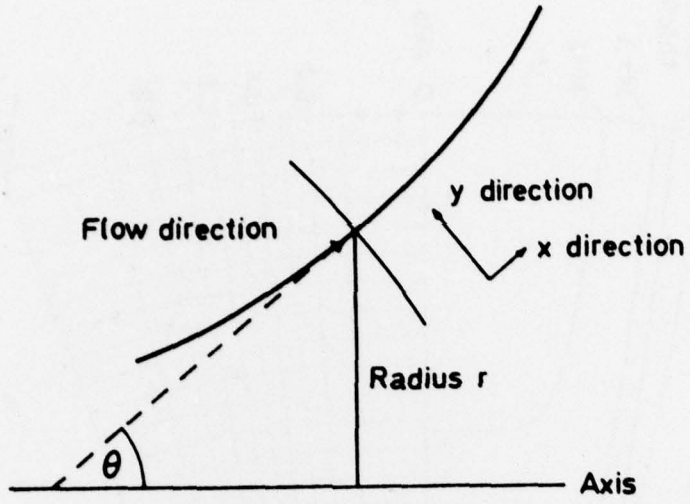

Fig 1 The coordinate system

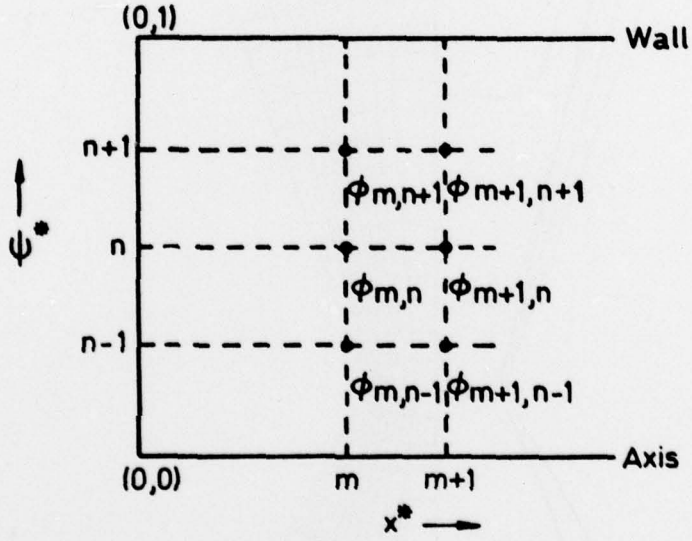

Fig 2 General point in the mesh scheme and domain of integration $x^*-\psi^*$ plane

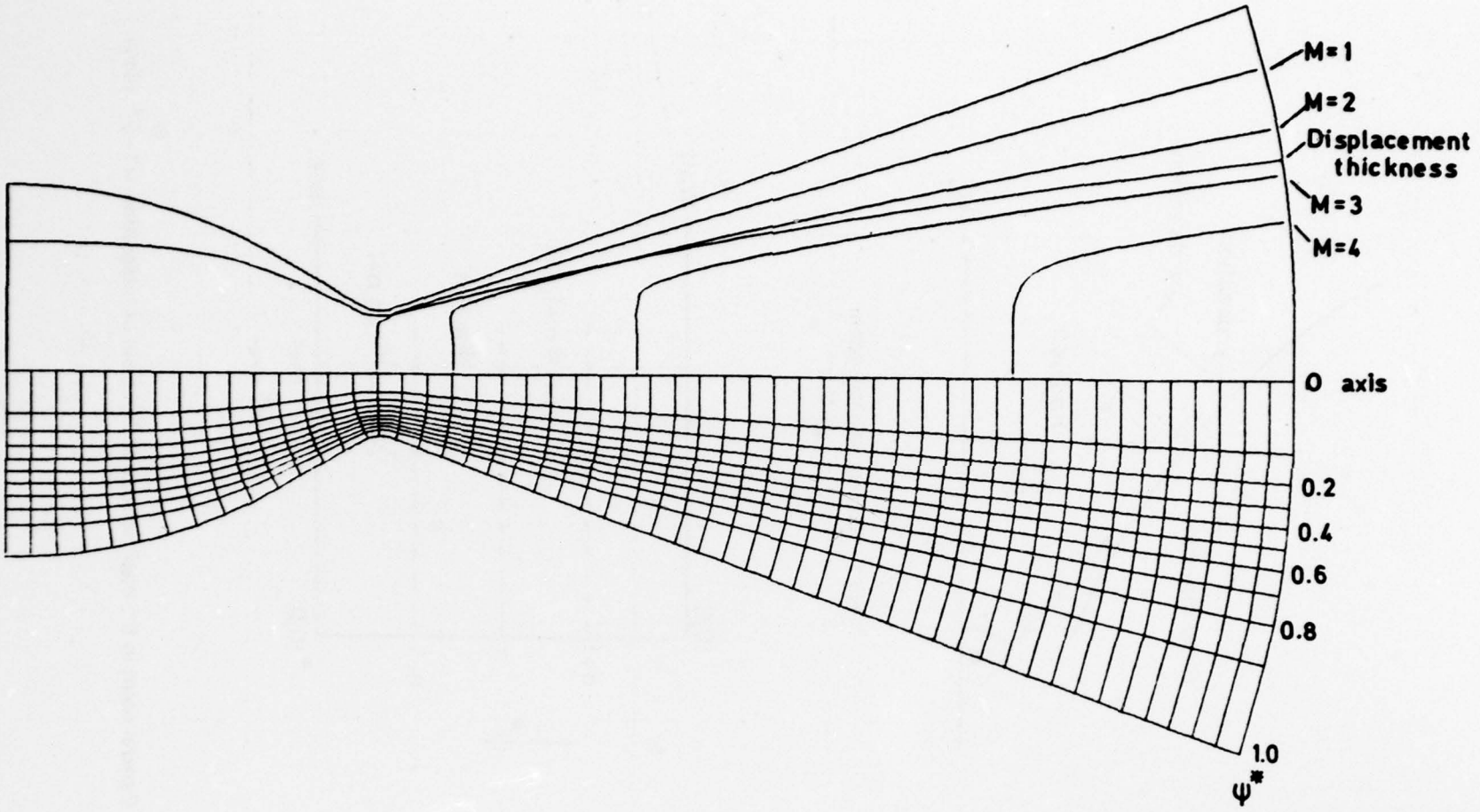

Fig 3 Computed flow field for example 1

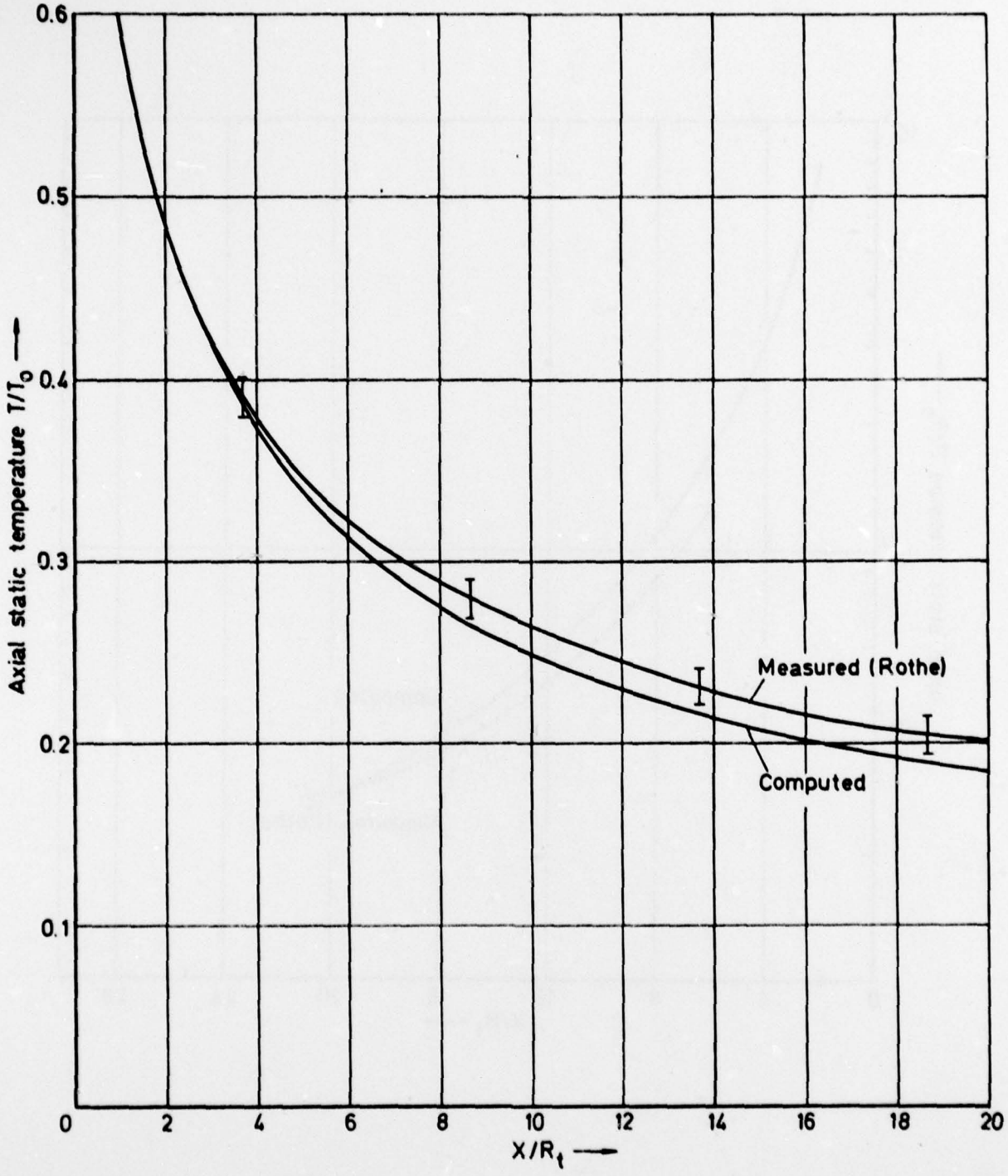

Fig 4 Axial static temperature: example 1

TR 77175

Fig 5

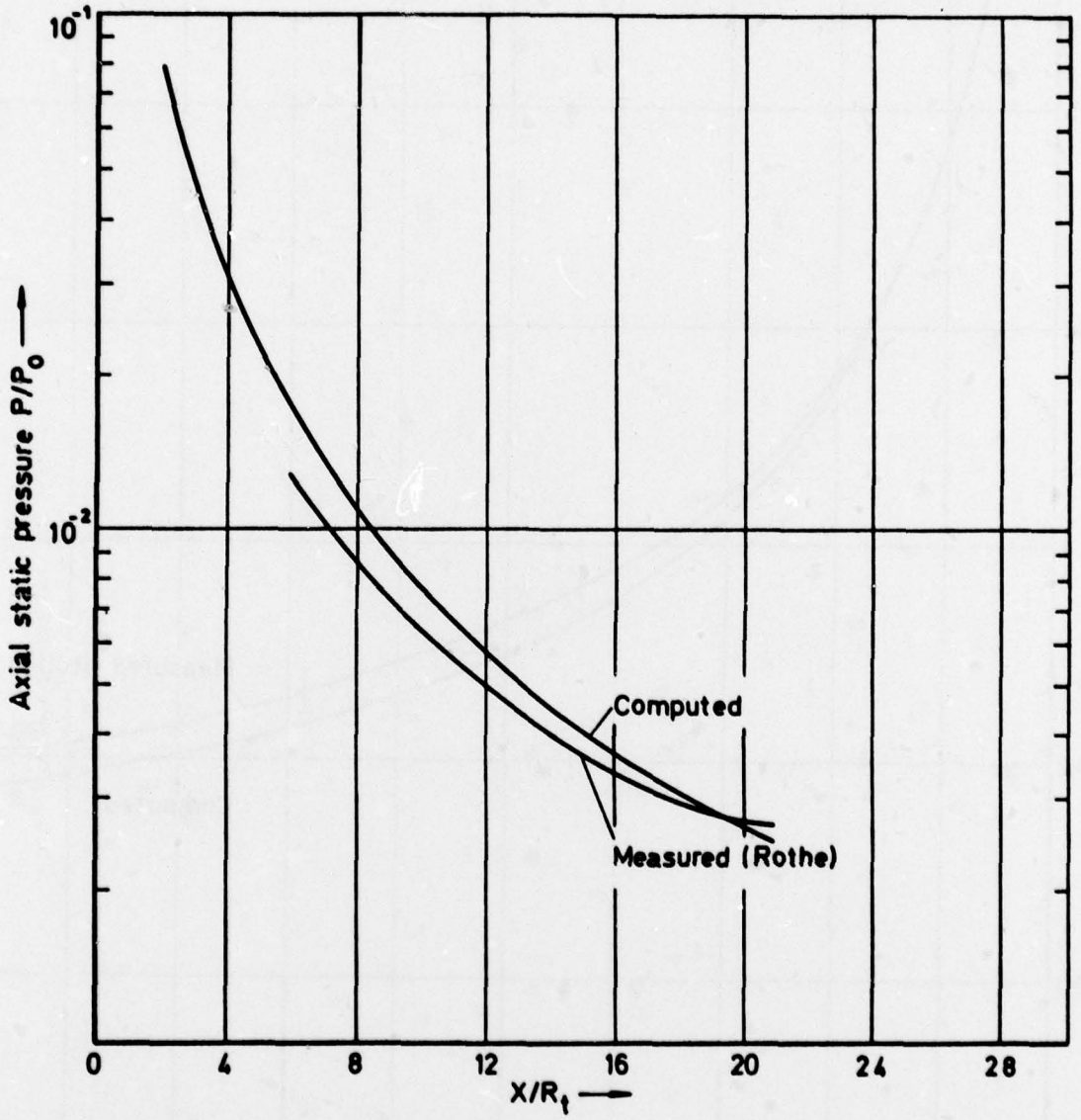

Fig 5 Axial static pressure: example 1

TR 77175

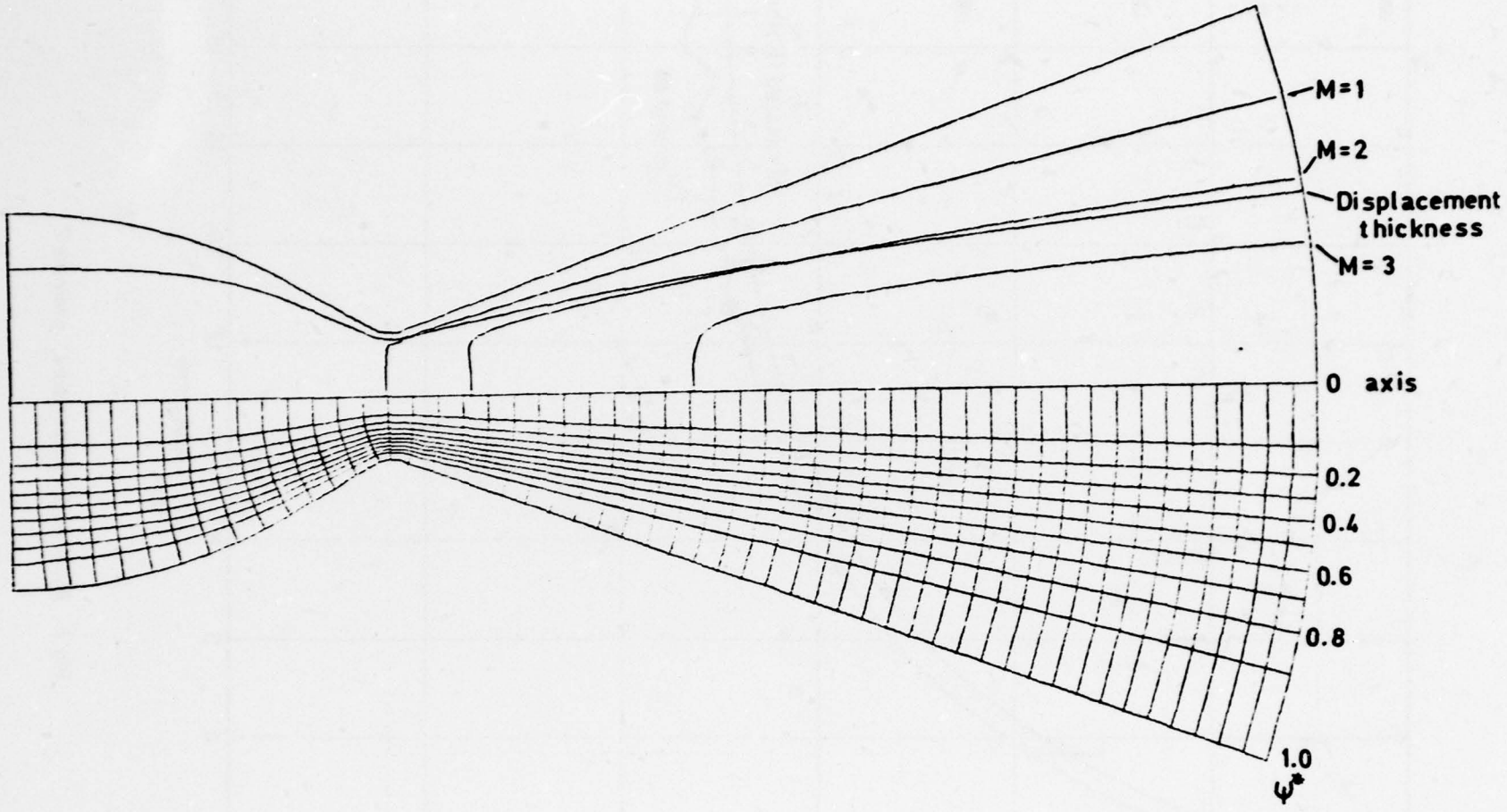

Fig 6 Computed flow field for example 2

Fig 7

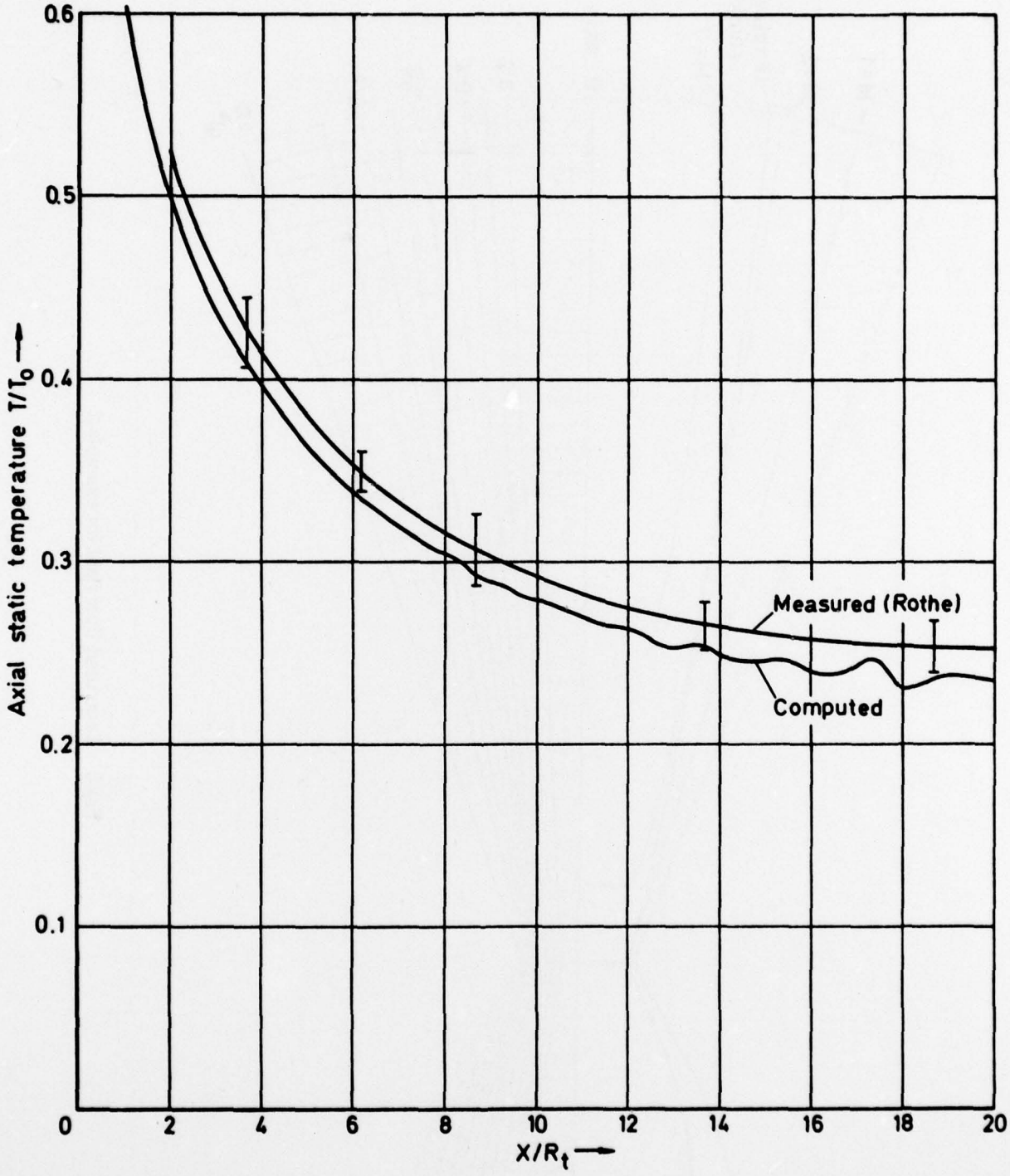

Fig 7 Axial static temperature: example 2

TR 77175

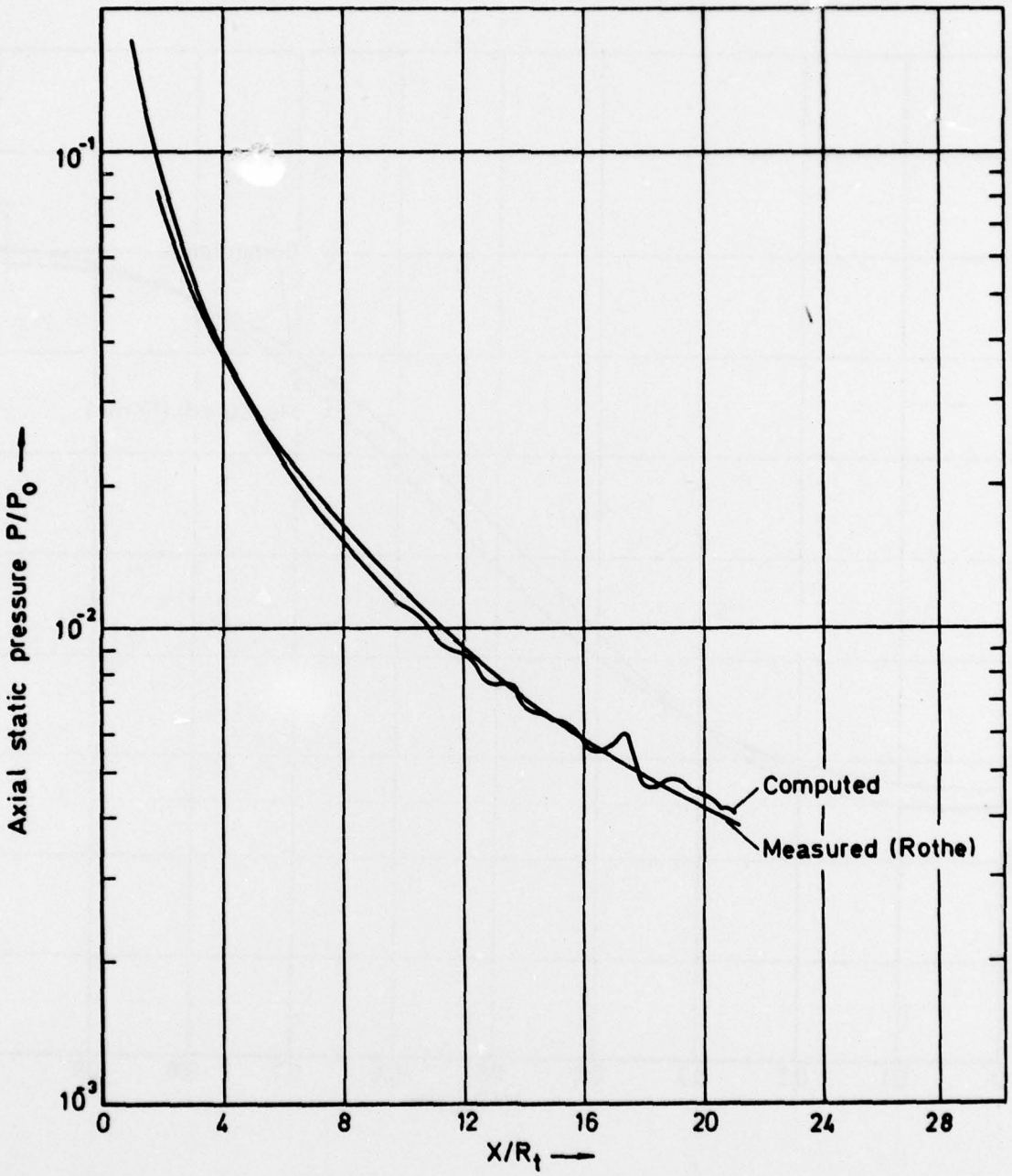

Fig 8 Axial static pressure: example 2

Fig 9

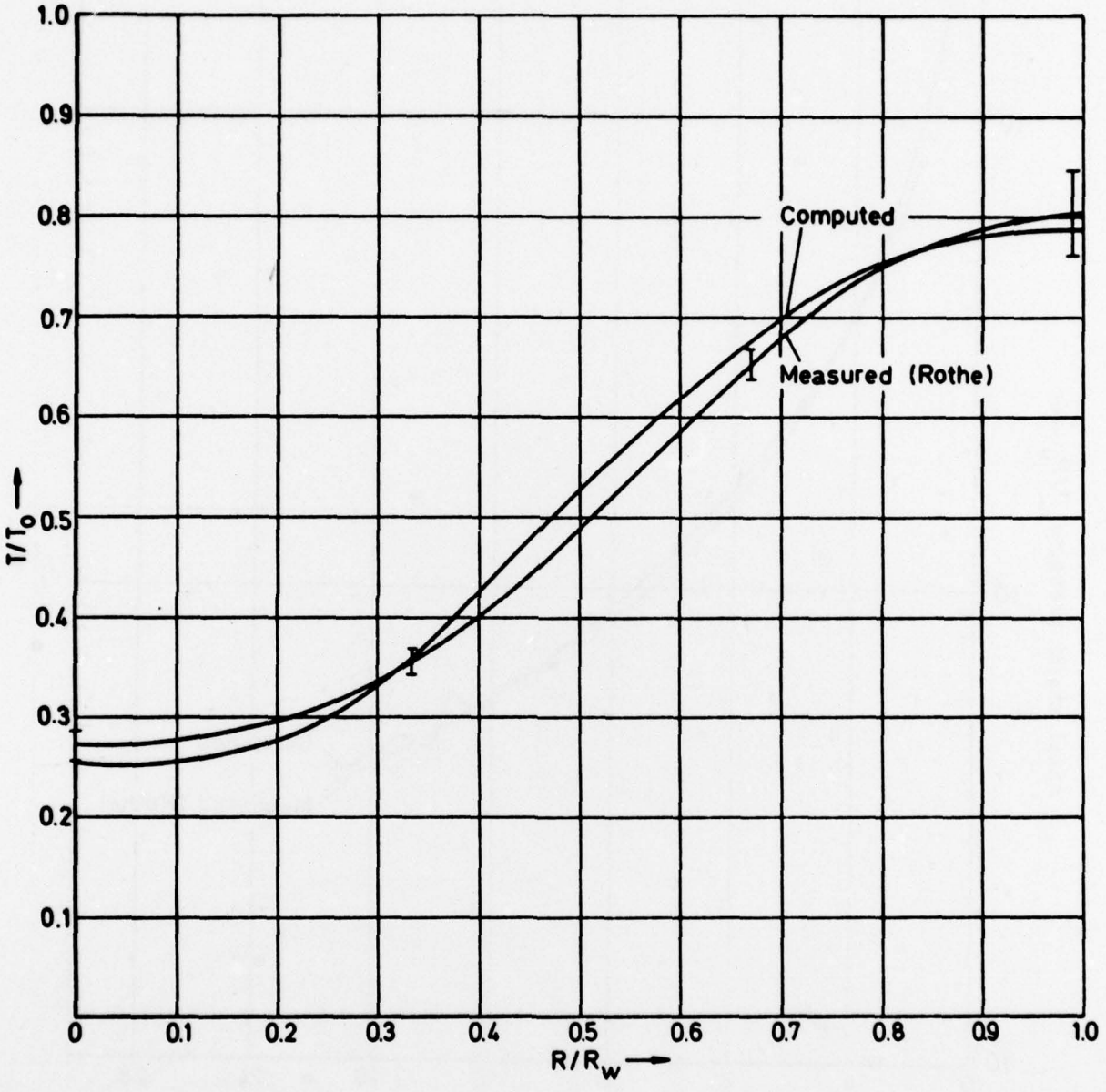

Fig 9 Non-dimensional static radial temperature at $X/R_t = 13.7$

TR 77175

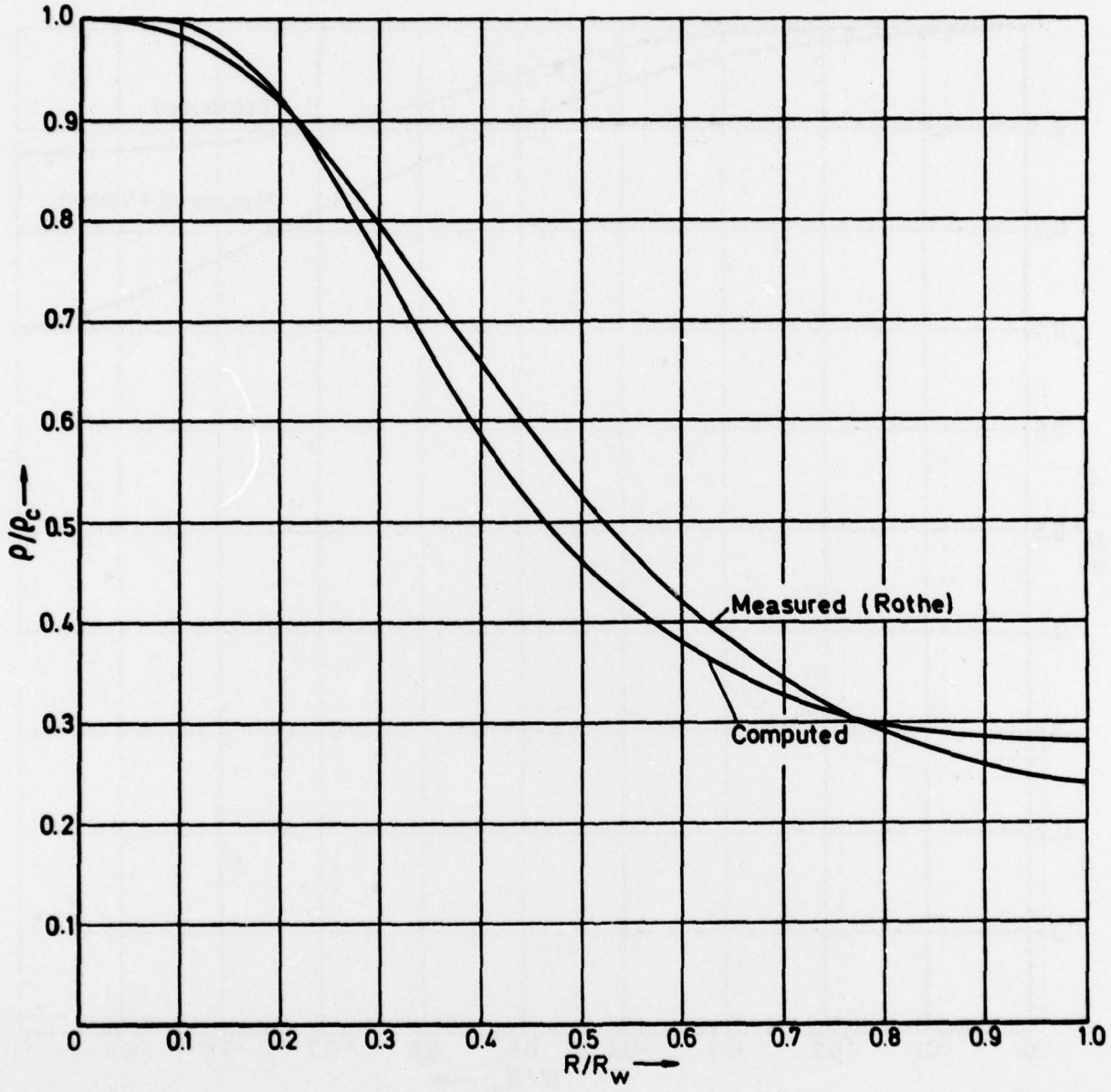

Fig 10 Normalised radial density at $X/R_t = 13.7$

Fig 11

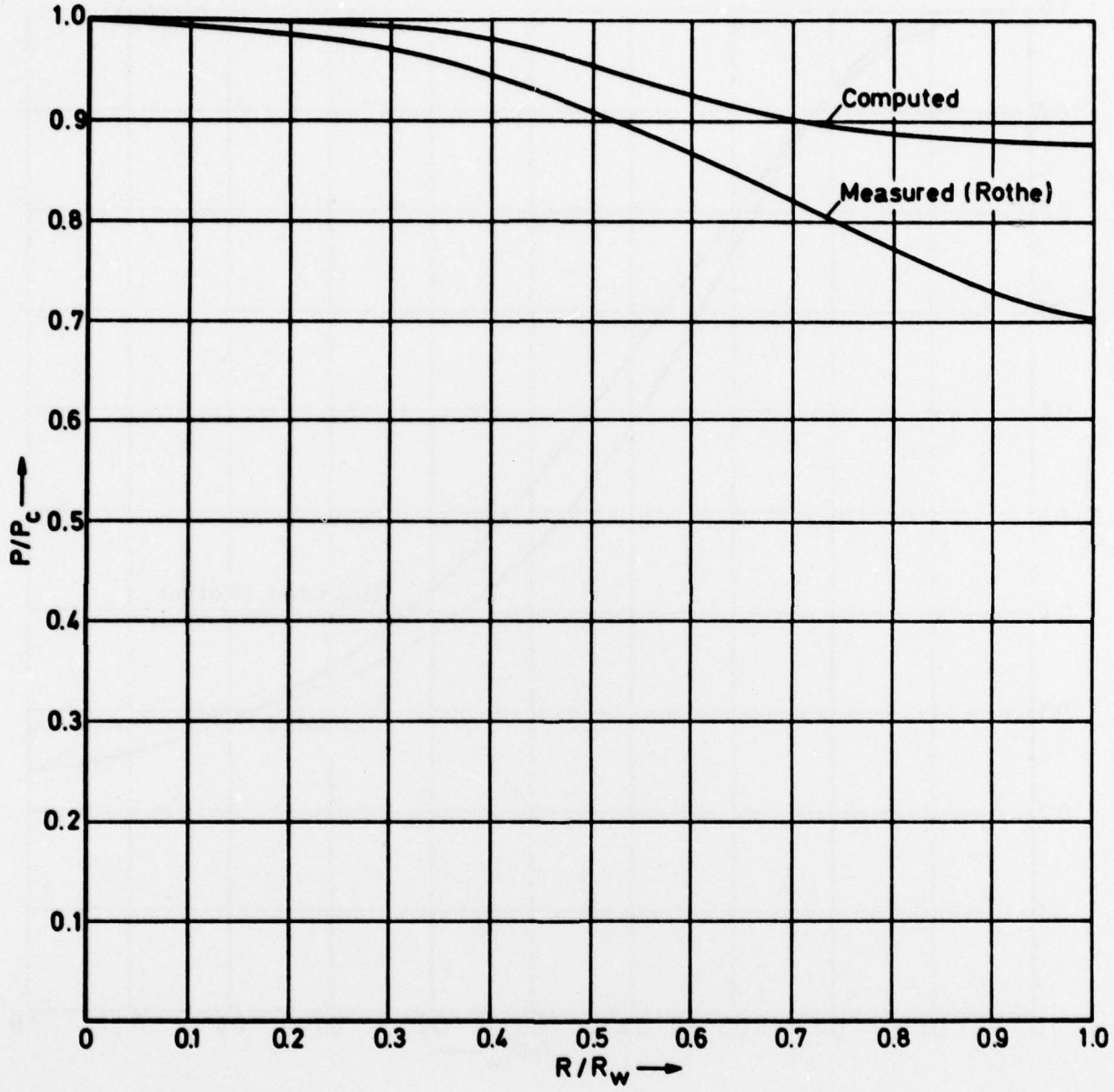

Fig 11 Normalised radial pressure at $X/R_t = 13.7$

TR 77175

REPORT DOCUMENTATION PAGE

Overall security classification of this page

UNCLASSIFIED

As far as possible this page should contain only unclassified information. If it is necessary to enter classified information, the box above must be marked to indicate the classification, e.g. Restricted, Confidential or Secret.

1. DRIC Reference (to be added by DRIC)	2. Originator's Reference	3. Agency Reference	4. Report Security Classification/Marking
BR-61832	RAE—TR-77175	N/A	UNCLASSIFIED

5. DRIC Code for Originator	6. Originator (Corporate Author) Name and Location
850100	Royal Aircraft Establishment, Farnborough, Hants, UK
5a. Sponsoring Agency's Code	**6a. Sponsoring Agency (Contract Authority) Name and Location**
N/A	N/A

7. Title: Laminar flow-field computation in axisymmetric nozzles

7a. (For Translations) Title in Foreign Language: Technical rept.

7b. (For Conference Papers) Title, Place and Date of Conference

8. Author 1. Surname, Initials	9a. Author 2	9b. Authors 3, 4	10. Date	Pages	Refs.
Barber, B.C.			Nov 77	33	19

11. Contract Number	12. Period	13. Project	14. Other Reference Nos.
N/A	N/A		Space 539

15. Distribution statement

(a) Controlled by – ~~MOD(PE) D Space~~

(b) Special limitations (if any) –

16. Descriptors (Keywords) (Descriptors marked * are selected from TEST)

Internal flow. Flow-field computation. Boundary layers. Nozzle flow.

17. Abstract

A numerical procedure for computing the laminar flow-field in nozzles at throat Reynolds numbers of 300-3000 is described. Such nozzles are found in space-craft position control thrusters, chemical lasers, and low density hypersonic wind-tunnels. A parabolic approximation of the Navier-Stokes equations (the boundary layer equations) is transformed to Von Mises form and solved numerically by a central difference method. The entire subsonic and supersonic flow-field is computed. No assumptions or approximations, other than those inherent in the flow equations, are involved. The method is of the direct type and the flow-field for any given nozzle geometry may, in principle, be computed. Examples are given comparing computed results with published experimental data.

310 45p

FS910/1

RAE Form A143